

Environment-Aware Channel Inference via Cross-Modal Flow: From Multimodal Sensing to Wireless Channels

Guangming Liang, *Graduate Student Member, IEEE*, Mingjie Yang, *Graduate Student Member, IEEE*, Dongzhu Liu, *Member, IEEE*, Paul Henderson, and Lajos Hanzo, *Life Fellow, IEEE*

Abstract—Accurate channel state information (CSI) underpins reliable and efficient wireless communication. However, acquiring CSI via pilot estimation incurs substantial overhead, especially in massive multiple-input multiple-output (MIMO) systems operating in high-Doppler environments. By leveraging the growing availability of environmental sensing data, this treatise investigates pilot-free channel inference that estimates complete CSI directly from multimodal observations, including camera images, LiDAR point clouds, and GPS coordinates. In contrast to prior studies that rely on predefined channel models, we develop a data-driven framework that formulates the sensing-to-channel mapping as a cross-modal flow matching problem. The framework fuses multimodal features into a latent distribution within the channel domain, and learns a velocity field that continuously transforms the latent distribution toward the channel distribution. To make this formulation tractable and efficient, we reformulate the problem as an equivalent conditional flow matching objective and incorporate a modality alignment loss, while adopting low-latency inference mechanisms to enable real-time CSI estimation. In experiments, we build a procedural data generator based on Sionna and Blender to support realistic modeling of sensing scenes and wireless propagation. System-level evaluations demonstrate significant improvements over pilot- and sensing-based benchmarks in both channel estimation accuracy and spectral efficiency for the downstream beamforming task.

Index Terms—Environment-aware communications, multimodal sensing, pilot-free channel estimation, generative AI, flow matching, dynamic wireless environments.

I. INTRODUCTION

As wireless networks evolve toward next generation (NG) systems, they are expected to support emerging applications such as immersive extended reality, digital twins, and holographic communications [1]. These applications require highly reliable yet low-latency communication links, which rely on accurate knowledge of the channel state information (CSI) to fully exploit the potential of massive multiple-input multiple-output (MIMO) technology [2]. However, acquiring high-resolution CSI for large-scale antenna arrays remains a major bottleneck, as traditional channel estimation methods introduce pilot overhead that scales with the number of antennas and user

terminals, thereby occupying spectral resources that could otherwise be used for data transmission. In simple tangible terms, the pilot overhead must be doubled every time the Doppler frequency is doubled. Consequently, significant research efforts have been devoted to reducing pilot overhead without sacrificing channel estimation accuracy [3]–[10]. Despite these advances, achieving accurate and low- or even zero-overhead CSI acquisition remains a key challenge in unlocking the full potential of massive MIMO in NG networks.

Environment-aware communications [11] have recently emerged as a promising paradigm to reduce or even eliminate reliance on pilot signals for CSI acquisition. By sensing environmental features, such as obstacle locations, reflector and scatterer characteristics, terrain and building layouts, and dynamic objects, communication systems can either directly infer channel states or predict propagation models characterized by path loss, shadowing, multipath, and LoS/NLoS conditions. This environmental awareness enables optimized transmission strategies, including beamforming, user scheduling, and resource allocation, without requiring explicit pilot-based CSI estimation. Existing studies on environment-aware communications generally follow a pair of representative strategies. The first one leverages multimodal sensing data, including GPS coordinates, camera RGB images, LiDAR point clouds, and radar signals, to perform channel-related downstream tasks such as beamforming design [12] and link-blockage detection [13]. Although this task-oriented approach bypasses explicit CSI estimation, the learned mappings are typically task-specific and lack generalization across system configurations. The second strategy relies solely on GPS-based localization to infer CSI under the assumptions of quasi-static environments [14], [15], which is inherently inapplicable to dynamic propagation scenarios.

To address the limitations discussed above, we propose a flow-matching-based generative framework that learns a continuous transformation from multimodal environmental sensing data to high-dimensional wireless channel states. This represents the first environment-aware technique capable of achieving real-time full CSI recovery from dynamic multimodal sensing data without relying on pilot signaling. By leveraging computational intelligence to replace communication overhead, the proposed framework enhances spectral efficiency, supports physical-layer operations facilitated by full CSI, and provides low-latency inference suitable for practical deployment in dynamic NG networks.

Guangming Liang, Mingjie Yang, Dongzhu Liu and Paul Henderson are with the School of Computing Science, University of Glasgow, Glasgow G12 8QQ, U.K, e-mails: {30322211,2921021y}@student.gla.ac.uk, {Dongzhu.Liu, Paul.Henderson}@glasgow.ac.uk. (Corresponding author: Dongzhu Liu.)

Lajos Hanzo is with the School of Electronics and Computer Science, University of Southampton, Southampton SO17 1BJ, U.K, e-mail: lh@ecs.soton.ac.uk.

TABLE I
CONTRASTING OUR CONTRIBUTIONS TO THE LITERATURE OF CHANNEL INFERENCE METHODS

	[3], [4]	[5]–[10]	[14]	[15]	[16]–[18]	Our work
Instantaneous CSI acquisition	✓	✓	✓	✓		✓
Pilot-free channel inference			✓	✓	✓	✓
No channel model assumption	✓	✓				✓
Machine-learning-based approach		✓		✓	✓	✓
Robustness to dynamic environment	✓	✓			✓	✓
Multimodal-sensing-based CSI estimation						✓
Flow-matching-based channel inference						✓
Real-time and low-latency requirement						✓

A. Related Works

1) *Channel Estimation with Reduced Pilot Overhead*: To mitigate the pilot overhead in massive MIMO systems, model-based [3], [4] and data-driven [5]–[10] methods have been proposed to reduce pilot usage, while preserving channel estimation accuracy. Model-based techniques, such as compressed sensing, exploit angular-domain sparsity to estimate high-dimensional CSI from limited pilot measurements [3], [4]. However, the sparsity assumption may not strictly hold in dynamic or rich-scattering environments, which limits their generalization capability. Data-driven methods aim to recover full CSI from partial estimates by capturing correlations across spatial, frequency, and temporal domains [5], [6] or by integrating auxiliary information such as historical CSI [7] and multi-view images [8]. Despite their effectiveness, these approaches often require large datasets and are typically tailored to specific pilot configurations, which limits their generalization to new scenarios. Recently, generative probabilistic models based on score matching [9] and diffusion processes [10] have been explored for learning the underlying channel distribution and estimate CSI through posterior sampling under arbitrary pilot settings. While these methods reduce pilot dependence, pilot-free CSI acquisition remains a radical open challenge, motivating the generative framework proposed in this paper.

2) *Environment-Aware Channel Inference*: Environmental sensing information has been increasingly exploited to enhance the understanding of wireless channels. Existing studies can be broadly categorized according to their underlying channel modeling assumptions. The first category assumes a statistical channel model and estimates its key parameters such as the path loss [16], Ricean K-factor [17], and root-mean-square delay spread [18] from multimodal sensing data, including GPS coordinates, RGB images, LiDAR point clouds, and radar signals. Instead of focusing on long-term statistical models, [14] assumes a quasi-static propagation environment, where the channel characteristics are inferred from spatial information using a K-nearest neighbors (KNN) approach that maps user locations to propagation path knowledge for reconstructing the MIMO channel coefficient matrix. Beyond conventional statistical or ray-tracing models, NeRF2 [15] learns a neural representation of radio propagation, effectively introducing a novel data-driven propagation mechanism that implicitly captures reflection, diffraction, and scattering effects to predict channel responses. While the above methods are capable of advanced environment-aware channel inference,

most of them are model-based and typically assume static environments or rely on single-modality inputs. By contrast, our work adopts a fully data-driven framework that infers complete CSI directly from multimodal sensing data, facilitating robust inference under dynamic wireless environments.

3) *Advances in Flow Matching for Distribution Mapping*: Recently, flow matching [19], [20] has emerged as a promising alternative to diffusion-based [21] and GAN-based [22] generative models. In contrast to diffusion models that rely on fixed Gaussian priors, flow matching provides a mathematically principled framework for learning continuous mappings between arbitrary distributions, covering both intramodal [23]–[25] and cross-modal [26]–[29] scenarios. In intra-modal settings (e.g., face-to-face [23], [24] and sketches-to-images [25] translations), flow matching learns a continuous transport process that maps one distribution to another. Extending this framework to cross-modal generation (e.g., text-to-image) is more challenging because the source and target reside in distinct data spaces. Early studies adopt Gaussian priors and condition the flow on auxiliary modality features (e.g., text embeddings) to guide this mapping [26], [27], which increases model complexity and often limits generative quality. To overcome these limitations, both CrossFlow [28] and FlowTok [29] project heterogeneous modalities into shared latent spaces, enabling more direct and efficient cross-modal distribution transformation. Despite these advances in computer vision, the potential of flow matching for supporting cross-modal distribution mapping in wireless communications, particularly for wireless channel inference, remains unexplored.

Our contributions are boldly and explicitly contrasted to the existing literature in Table I and are further described next.

B. Contributions and Organization

This work investigates environment-aware channel inference in dynamic wireless environments, where we infer complete CSI directly from multimodal sensing data, including camera images, LiDAR point clouds, and GPS coordinates, without relying on pilot signaling. Building on recent advances in flow-based generative modeling, we develop a cross-modal flow matching framework that bridges the distributions of multimodal sensing data and channel representations to enable real-time and model-free CSI estimation. In contrast to prior sensing-enabled communication approaches tailored to specific tasks such as beamforming, our framework consequently generalizes to downstream physical-layer operations and provides a unified foundation for multimodal sensing

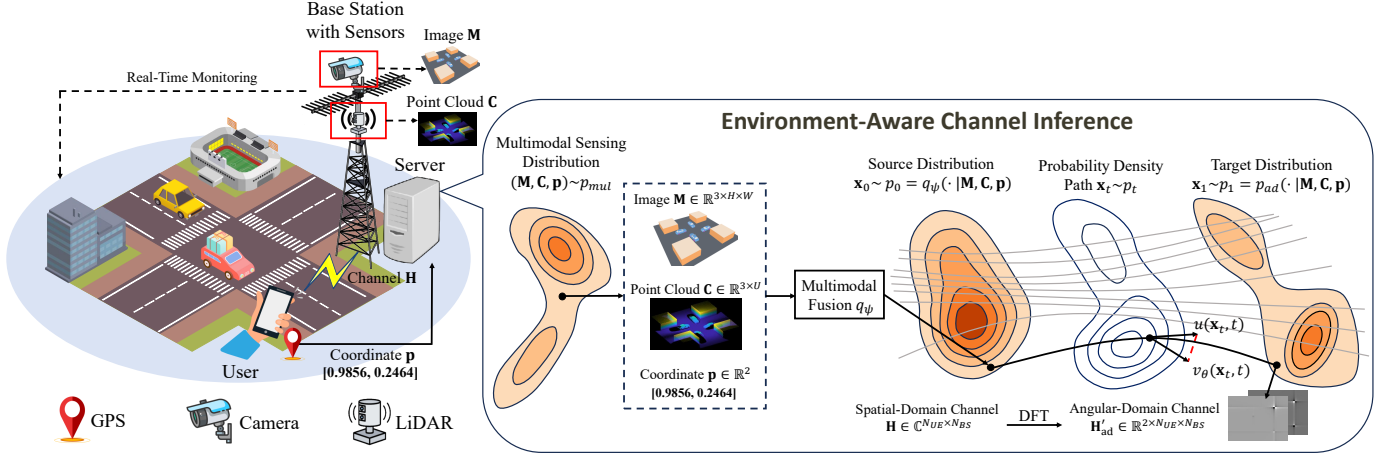


Fig. 1. Physical scenario where the base station is equipped with a camera, a LiDAR system and a server, and the user is deployed with a GPS. At the server, the complete CSI between the base station and the user is estimated from multimodal sensing data, including image, point cloud and coordinate.

and communication integration. The main contributions are summarized below.

- **Modeling environment-aware channel inference via cross-modal flow:** We model environment-aware channel inference as a cross-modal flow matching problem [28], [29], where the transformation from multimodal sensing distribution to wireless channel distribution is represented as a continuous cross-modal flow. To realize this flow, heterogeneous sensing modalities are fused through a stochastic encoder into a multimodal latent distribution in the channel space. Then, the model learns a time-dependent velocity field that drives the evolution from the fused sensing modalities toward the target channel modality. This formulation serves as the basis for the subsequent learning and inference framework.

- **Tractable learning and efficient inference design:** To make the proposed formulation tractable, we reformulate it as a conditional flow matching problem that learns the velocity field conditioned on the accessible samples drawn from the encoded multimodal latent (source) and wireless channel (target) distributions. To reduce the mismatch between the two distributions, we introduce a modality alignment loss that not only regularizes the encoded source distribution but encourages it to closely align with the target channel distribution. During inference, a second-order numerical integration scheme is employed to approximate the learned cross-modal flow for reducing latency and preserve estimation quality.

- **Experiments:** We construct a procedural data generator based on Sionna [30] and Blender [31] to enable the joint modeling of realistic sensing environments and wireless propagation. System-level experiments show that the proposed framework achieves sub -10 dB normalized mean square error (NMSE) in channel estimation and up to 25% improvement in spectral efficiency for beamforming as a downstream task, outperforming both pilot-based and sensing-based baselines, while generalizing beyond task-specific multimodal beamforming.

The remainder of the paper is organized as follows. Section II introduces the system model. Section III presents our problem formulation for environment-aware channel inference. The

learning and optimization framework is presented in Section VI. Section V provides experimental results, followed by our conclusions in Section VI.

II. SYSTEM MODEL

A. Physical Scenario and Transmission Protocol

As shown in Fig. 1, we consider a massive MIMO system operating in the millimeter wave (mmWave) band, where a base station (BS) having N_{BS} transmit antennas (TAs) serves a single user equipped with N_{UE} receive antennas (RAs).¹ The coverage region includes both static and dynamic entities, such as buildings and moving vehicles, which affect the propagation of electromagnetic signals. To enable real-time monitoring of the wireless environment, the BS is equipped with a LiDAR sensor, a panoramic camera, and it also receives GPS information reported by the associated user. Specifically, the LiDAR point cloud, consisting of U three-dimensional points, is denoted as $\mathbf{C} \in \mathbb{R}^{3 \times U}$, which characterizes the spatial structure of the environment, including the shape, size, and distance of surrounding objects. The panoramic camera image having a height H , width W , and RGB channels is denoted as $\mathbf{M} \in \mathbb{R}^{3 \times H \times W}$, which captures a 360-degree view of the environment. The two-dimensional GPS coordinate is denoted as $\mathbf{p} \in \mathbb{R}^2$, representing the position relative to the BS. All these multimodal sensing data are collected and stored at the server deployed at the BS. In this paper, we aim to infer complete CSI between the BS and the user from multimodal sensing data, a task referred to as environment-aware channel inference. This method completely obviates the need for pilot signals in CSI acquisition and therefore saves valuable spectral resources, while being less susceptible to channel impairments (e.g., additive Gaussian white noise) and pilot-related limitations (e.g., insufficient pilot length) compared to conventional pilot-based approaches.

¹For simplicity but without loss of generality, a single-user MIMO system is considered in this work. However, the results can be easily extended to multi-user scenarios by utilizing orthogonal resource allocation and linear precoding techniques.

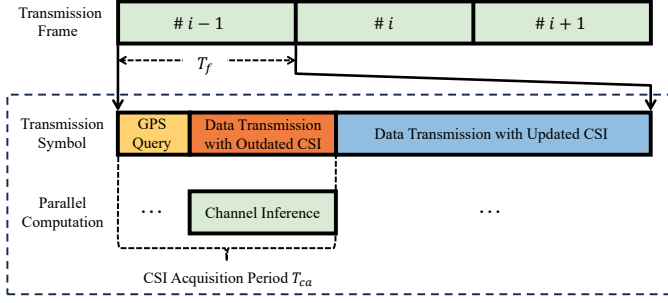


Fig. 2. Transmission protocol with frame-based CSI acquisition, where the environment-aware channel inference is employed for CSI update.

The transmission protocol is illustrated in Fig. 2, where environment-aware channel inference is employed for CSI acquisition. The transmission resources are divided into consecutive frames, each with a duration of T_f . We assume a block-fading channel model in which the CSI remains constant within each frame but varies randomly and independently across frames. Each transmission frame starts with a CSI acquisition period T_{ca} , during which the user reports its instantaneous coordinate to the BS in the GPS query phase. This phase is followed by a channel inference stage, when the BS infers the CSI of the current block by exploiting the reported position together with the camera image and LiDAR point cloud, while data transmission continues concurrently using the outdated CSI from the previous frame. Once the inference is completed, the updated CSI is applied for the rest of the frame.

B. Channel Representation and Pre/Post-Processing

We denote the mmWave MIMO channel between the BS and the user by $\mathbf{H} \in \mathbb{C}^{N_{UE} \times N_{BS}}$. Due to the limited number of propagation clusters and the narrow angular spread, the mmWave channel exhibits sparsity in the angular domain. Motivated by this observation and following [32], we perform channel inference in the angular domain. To this end, the spatial-domain channel matrix \mathbf{H} is transformed into its angular-domain counterpart \mathbf{H}_{ad} through discrete Fourier transforms (DFT) as

$$\mathbf{H}_{ad} = \mathbf{F}_{N_{UE}}^H \mathbf{H} \mathbf{F}_{N_{BS}}, \quad (1)$$

where $\mathbf{F}_{N_{UE}} \in \mathbb{C}^{N_{UE} \times N_{UE}}$ and $\mathbf{F}_{N_{BS}} \in \mathbb{C}^{N_{BS} \times N_{BS}}$ represent the DFT matrices defined as

$$[\mathbf{F}_{N_{UE}}]_{m,k} = \frac{1}{\sqrt{N_{UE}}} e^{j \frac{2\pi}{N_{UE}} (m-1)(k-1)}, \quad m, k = 1, \dots, N_{UE}, \quad (2)$$

$$[\mathbf{F}_{N_{BS}}]_{m,k} = \frac{1}{\sqrt{N_{BS}}} e^{j \frac{2\pi}{N_{BS}} (m-1)(k-1)}, \quad m, k = 1, \dots, N_{BS}. \quad (3)$$

Since conventional neural networks operate on real-valued tensors, the complex angular-domain channel matrix \mathbf{H}_{ad} is converted into a real-valued representation before being fed into the learning model. Specifically, we stack its real and imaginary components along the first dimension to form $\mathbf{H}'_{ad} \in \mathbb{R}^{2 \times N_{UE} \times N_{BS}}$. After inference, the resultant real-valued tensor $\widehat{\mathbf{H}}'_{ad}$ is transformed back into its complex form as

$$\widehat{\mathbf{H}}_{ad} = \widehat{\mathbf{H}}'_{ad}(1, :, :) + j \widehat{\mathbf{H}}'_{ad}(2, :, :), \quad (4)$$

yielding the estimated angular-domain channel matrix. Then, the estimated channel $\widehat{\mathbf{H}}$ in the spatial domain is obtained by the inverse DFT operation

$$\widehat{\mathbf{H}} = \mathbf{F}_{N_{UE}} \widehat{\mathbf{H}}_{ad} \mathbf{F}_{N_{BS}}^H. \quad (5)$$

III. PROBLEM FORMULATION FOR ENVIRONMENT-AWARE CHANNEL INFERENCE

As established in channel modeling studies, the wireless channel between a transmitter and a receiver is primarily determined by their relative geometry and the surrounding environment [33]. This intrinsic dependency provides a physical basis for inferring high-dimensional channel matrices from multimodal environmental sensing data.

To capture this dependency, we model both the multimodal environmental sensing data and the wireless channel as random variables that follow different probability distributions. Specifically, the sensing distribution characterizes the stochastic variations in LiDAR, camera, and the GPS data gleaned from different environmental configurations, while the channel distribution represents the corresponding variations in the channel matrices. This distributional formulation naturally fits within the flow matching framework [19], which models data generation as a continuous transformation from a source to a target distribution guided by a velocity field.

However, in environment-aware channel inference, the source and target distributions correspond to heterogeneous modalities lying in different data spaces, which makes standard flow matching formulations inapplicable [19], [20]. To generalize flow matching to this setting, we propose a cross-modality evolution framework, where heterogeneous sensing modalities are fused into a shape-aligned channel space to form a latent distribution. Then, a mapping between this latent distribution and the target channel distribution is learned. This framework is conceptually related to the CrossFlow [28], which adapts flow matching to a cross-domain generation task (i.e., text-to-image), but differs fundamentally in that our goal is to infer the wireless channel representation from multimodal environmental sensing data.

As illustrated in Fig. 1, we formalize the environment-aware channel inference problem by considering multimodal sensing-channel observations $(\mathbf{M}, \mathbf{C}, \mathbf{p}, \mathbf{H}'_{ad})$ jointly drawn from an environmental distribution

$$p_{\text{env}}(\mathbf{M}, \mathbf{C}, \mathbf{p}, \mathbf{H}'_{ad}) = p_{\text{mul}}(\mathbf{M}, \mathbf{C}, \mathbf{p}) p_{\text{ad}}(\mathbf{H}'_{ad} | \mathbf{M}, \mathbf{C}, \mathbf{p}), \quad (6)$$

where $p_{\text{mul}}(\mathbf{M}, \mathbf{C}, \mathbf{p})$ denotes the joint distribution of multimodal sensing observations. The camera RGB image \mathbf{M} , LiDAR point cloud \mathbf{C} , and GPS coordinate \mathbf{p} are fused through a stochastic encoder q_ψ having learnable parameters ψ , yielding a conditional latent distribution $q_\psi(\cdot | \mathbf{M}, \mathbf{C}, \mathbf{p})$ that serves as the source distribution p_0 . Conditioned on the same multimodal sensing observations, the conditional channel distribution $p_{\text{ad}}(\cdot | \mathbf{M}, \mathbf{C}, \mathbf{p})$ functions as the target distribution p_1 . The continuous transformation from the source distribution p_0 to the target distribution p_1 is described by a probability path $\{p_t\}_{t \in [0,1]}$ that smoothly interpolates between them. This path is governed by a time-dependent velocity field $u(\mathbf{x}, t)$, so

that the evolution of an intermediate state $\mathbf{x}_t \sim p_t$ follows the ordinary differential equation (ODE)

$$\frac{d\mathbf{x}_t}{dt} = u(\mathbf{x}_t, t), \quad (7)$$

which characterizes the instantaneous flow that is capable of transporting samples from the multimodal latent distribution q_ψ toward the channel distribution p_{ad} . Since the true velocity field $u(\mathbf{x}_t, t)$ implied by the probability path is generally intractable, we approximate it using a neural network $v_\theta(\mathbf{x}_t, t)$ relying on the learnable parameters θ . Following the standard flow matching formulation in [19], the learning objective is to minimize the expected discrepancy between the neural and true velocity fields:

$$(P1) \quad \min_{\psi, \theta} \mathcal{J}_{\text{FM}} = \mathbb{E}_{t \sim \mathcal{U}[0,1], \mathbf{x}_t \sim p_t} \|v_\theta(\mathbf{x}_t, t) - u(\mathbf{x}_t, t)\|_F^2. \quad (8)$$

IV. LEARNING AND OPTIMIZATION FOR ENVIRONMENT-AWARE CHANNEL INFERENCE

In this section, we propose a cross-modal flow matching framework to realize environment-aware channel inference. Specifically, we introduce the learning objectives for cross-modal flow matching in Sec. IV-A, describe the model architecture and parameterization in Sec. IV-B, and elaborate on the optimization and inference pipeline in Sec. IV-C.

A. Learning Objectives for Cross-Modal Flow Matching

To achieve environment-aware channel inference, we design learning objectives for tractable cross-modal flow matching. Specifically, we reformulate the original flow matching objective in (8) to enable Monte Carlo approximation, and introduce an extra modality alignment loss for supporting the evolution from multimodal sensing data toward the channel representation. Finally, the overall learning objective is proposed.

1) *Flow Matching Loss Reformulation:* Although the flow matching objective in (8) provides a theoretically elegant formulation, it is intractable to use in practice. This is because the true probability path p_t and its corresponding velocity field $u(\mathbf{x}_t, t)$ are unknown and cannot be explicitly constructed without access to the underlying generative process that transforms p_0 to p_1 . In other words, during model training, we can only observe the initial state \mathbf{x}_0 and the terminal state \mathbf{x}_1 from the source latent distribution q_ψ (i.e., p_0) and the target channel distribution p_{ad} (i.e., p_1), respectively, but we have no prior knowledge of an appropriate pair $[p_t, u(\mathbf{x}_t, t)]$ that yields a continuous flow to connect them. To address this issue, we construct a conditional probability path $p_t(\mathbf{x}_t; \mathbf{x}_0, \mathbf{x}_1)$ and a corresponding conditional velocity field $u(\mathbf{x}_t, t; \mathbf{x}_0, \mathbf{x}_1)$, which describe the evolution of intermediate states \mathbf{x}_t conditioned on the accessible paired sensing-channel representations $(\mathbf{x}_0, \mathbf{x}_1)$ drawn from a joint distribution, formally defined as

$$(\mathbf{x}_0, \mathbf{x}_1) \sim \pi(\mathbf{x}_0, \mathbf{x}_1), \quad (9)$$

whose marginal distributions are q_ψ and p_{ad} , respectively.

To make the conditional path $p_t(\mathbf{x}_t; \mathbf{x}_0, \mathbf{x}_1)$ analytically tractable, we follow [20] and model it as an element-wise Gaussian distribution with mean $t\mathbf{x}_1 + (1-t)\mathbf{x}_0$ and isotropic

variance σ_{\min}^2 , implying element-wise independence within \mathbf{x}_t . The marginal probability path can be obtained by integrating out the joint distribution of the initial and terminal states:

$$p_t(\mathbf{x}_t) = \int p_t(\mathbf{x}_t; \mathbf{x}_0, \mathbf{x}_1) \pi(\mathbf{x}_0, \mathbf{x}_1) d\mathbf{x}_0 d\mathbf{x}_1. \quad (10)$$

Given the definition of $p_t(\mathbf{x}_t; \mathbf{x}_0, \mathbf{x}_1)$, its mean reduces to \mathbf{x}_0 and \mathbf{x}_1 at $t = 0$ and $t = 1$, respectively. Substituting these endpoint cases into (10) shows that the marginal distributions at the boundaries correspond to Gaussian-smoothing of the source and target distributions, i.e.,

$$p_0 = q_\psi * \mathcal{N}_{\text{iid}}(0, \sigma_{\min}^2), \quad p_1 = p_{\text{ad}} * \mathcal{N}_{\text{iid}}(0, \sigma_{\min}^2), \quad (11)$$

where $*$ denotes convolution over the tensor domain. As $\sigma_{\min} \rightarrow 0$, the marginal distributions converge to $p_0 = q_\psi$ and $p_1 = p_{\text{ad}}$, which are the desired source and target distributions defined in the problem formulation.

Having established the conditional probability path that satisfies the desired marginal conditions, we next derive the corresponding conditional velocity field through the ODE in (7). According to the definition of conditional Gaussian path, the intermediate state $\mathbf{x}_t \sim p_t(\mathbf{x}_t; \mathbf{x}_0, \mathbf{x}_1)$ can be represented as

$$\mathbf{x}_t = t\mathbf{x}_1 + (1-t)\mathbf{x}_0 + \sigma_{\min}\boldsymbol{\epsilon}, \quad (12)$$

where the elements of $\boldsymbol{\epsilon}$ are independently and identically distributed (i.i.d.) as $\mathcal{N}(0, 1)$. Taking the time derivative of (12) yields the conditional velocity field as follows:

$$\begin{aligned} u(\mathbf{x}_t, t; \mathbf{x}_0, \mathbf{x}_1) &= \frac{d}{dt}((1-t)\mathbf{x}_0 + t\mathbf{x}_1 + \sigma_{\min}\boldsymbol{\epsilon}) \\ &= \mathbf{x}_1 - \mathbf{x}_0. \end{aligned} \quad (13)$$

Given the conditional probability path $p_t(\mathbf{x}_t; \mathbf{x}_0, \mathbf{x}_1)$ and velocity field $u(\mathbf{x}_t, t; \mathbf{x}_0, \mathbf{x}_1)$, we extend the original flow matching objective in (8) by replacing the probability path and velocity field with their conditional counterparts and introducing an expectation over the joint distribution $\pi(\mathbf{x}_0, \mathbf{x}_1)$. The resultant conditional flow matching (CFM) objective is given as follows:

$$\begin{aligned} \mathcal{J}_{\text{CFM}} &= \mathbb{E}_{t \sim \mathcal{U}[0,1], (\mathbf{x}_0, \mathbf{x}_1) \sim \pi, \mathbf{x}_t \sim p_t(\cdot; \mathbf{x}_0, \mathbf{x}_1)} \|v_\theta(\mathbf{x}_t, t) - u(\mathbf{x}_t, t; \mathbf{x}_0, \mathbf{x}_1)\|_F^2, \\ &\stackrel{\sigma_{\min} \rightarrow 0}{=} \mathbb{E}_{t \sim \mathcal{U}[0,1], (\mathbf{x}_0, \mathbf{x}_1) \sim \pi} \|v_\theta(t\mathbf{x}_1 + (1-t)\mathbf{x}_0, t) - (\mathbf{x}_1 - \mathbf{x}_0)\|_F^2, \end{aligned} \quad (14)$$

where the second equality follows from the representation of \mathbf{x}_t in (12) as $\sigma_{\min} \rightarrow 0$. It has been shown in [19], [20] that the conditional formulation in (14) achieves the same gradient dynamics as the original flow matching objective in (8), i.e., $\nabla \mathcal{J}_{\text{FM}} = \nabla \mathcal{J}_{\text{CFM}}$. This indicates that conditional flow matching provides a tractable yet theoretically equivalent alternative to the intractable original formulation, which enables efficient optimization of θ and ψ via (14).

In particular, we model the latent distribution $q_\psi(\mathbf{x}_0 | \mathbf{M}, \mathbf{C}, \mathbf{p})$ as a multivariate Gaussian distribution with mean $\boldsymbol{\mu}(\mathbf{M}, \mathbf{C}, \mathbf{p}; \psi) \in \mathbb{R}^{2 \times N_{\text{UE}} \times N_{\text{BS}}}$ and standard deviation $\boldsymbol{\sigma}(\mathbf{M}, \mathbf{C}, \mathbf{p}; \psi) \in \mathbb{R}_{\geq 0}^{2 \times N_{\text{UE}} \times N_{\text{BS}}}$, where both $\boldsymbol{\mu}$ and $\boldsymbol{\sigma}$ are outputs of a neural network parameterized by ψ with inputs $(\mathbf{M}, \mathbf{C}, \mathbf{p})$. Using the reparameterization technique, the initial state is sampled as

$$\mathbf{x}_0 = \boldsymbol{\mu}(\mathbf{M}, \mathbf{C}, \mathbf{p}; \psi) + \boldsymbol{\sigma}(\mathbf{M}, \mathbf{C}, \mathbf{p}; \psi) \odot \boldsymbol{\epsilon}, \quad (15)$$

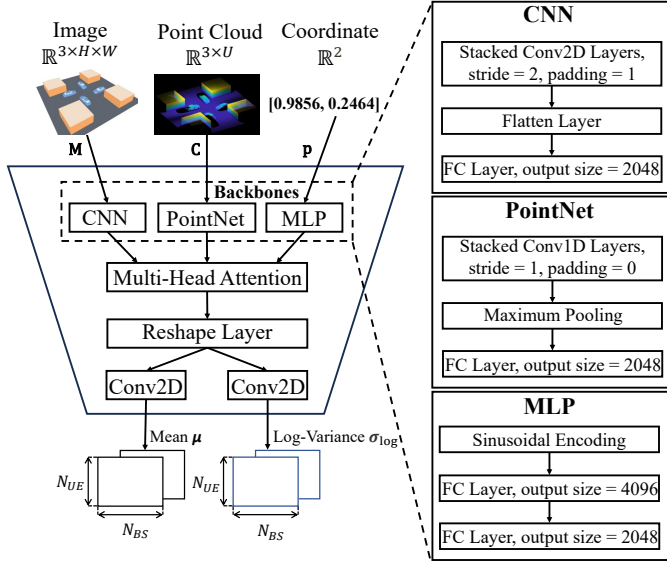


Fig. 3. Network structure of the multimodal stochastic encoder.

where the elements of ϵ are i.i.d. as $\mathcal{N}(0, 1)$ and \odot denotes element-wise multiplication. Given a batch of paired multimodal sensing-channel samples $\{\mathbf{M}^{[s]}, \mathbf{C}^{[s]}, \mathbf{p}^{[s]}, \mathbf{H}_{\text{ad}}^{[s]}\}_{s=1}^S$ and time indices $\{t^{[s]}\}_{s=1}^S$ independently sampled from the uniform distribution $\mathcal{U}[0, 1]$, we approximate the expectation in (14) via Monte Carlo sampling, and thus, obtain the empirical conditional flow matching loss:

$$\mathcal{L}_{\text{CFM}} = \frac{1}{S} \sum_{s=1}^S \left\| v_{\theta}(t^{[s]} \mathbf{H}_{\text{ad}}^{[s]} + (1 - t^{[s]}) \mathbf{x}_0^{[s]}, t^{[s]}) - (\mathbf{H}_{\text{ad}}^{[s]} - \mathbf{x}_0^{[s]}) \right\|_F^2. \quad (16)$$

2) Modality Alignment Loss: In sensing-to-channel flow, training the stochastic encoder solely with the conditional flow matching loss often leads to a highly uneven source distribution, while the induced probability path toward the target channel distribution may become unnecessarily irregular, which unavoidably degrades the generative performance. To ensure efficient transport, our goal is to identify the minimal and smoothest path that connects the source and target distributions, which can be theoretically interpreted as maximizing their mutual information. In practice, it is equivalent to minimizing the contrastive loss, which attracts paired multimodal sensing-channel samples while repelling unpaired ones, as pointed out in [34]. By enforcing stronger alignment between the multimodal latent representations and channel matrices, the resultant transport paths achieve improved smoothness and efficiency, which facilitates faster convergence and enhances stability of the flow matching process.

Motivated by this principle, we design the *modality alignment loss* that jointly minimizes the contrastive loss to enhance cross-modal consistency and incorporates a KL-divergence term to regularize the encoded source distribution:

$$\mathcal{L}_{\text{MA}} = -\frac{1}{S} \sum_{s=1}^S \log \frac{\exp(\text{sim}(\mathbf{x}_0^{[s]}, \mathbf{H}_{\text{ad}}^{[s]})/\tau)}{\sum_{k=1}^S \exp(\text{sim}(\mathbf{x}_0^{[s]}, \mathbf{H}_{\text{ad}}^{[k]})/\tau)} + \lambda \mathcal{L}_{\text{KL}}, \quad (17)$$

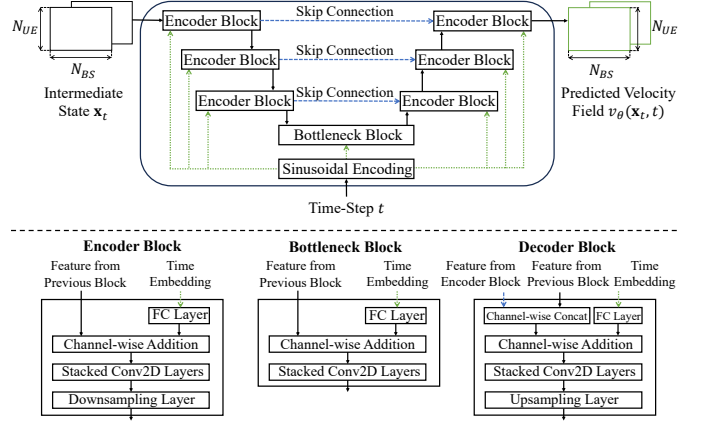


Fig. 4. Network structure of the neural velocity field.

where τ denotes the trainable temperature coefficient controlling the contrastive sharpness, λ is the hyperparameter that balances the alignment and regularization terms, and $\text{sim}(\cdot, \cdot)$ represents the cosine similarity, while the KL-divergence loss is defined as

$$\mathcal{L}_{\text{KL}} = -\frac{1}{S} \sum_{s=1}^S \mathbf{1}^T \text{vec} \left(1 + \log \left(\sigma^2(\mathbf{M}^{[s]}, \mathbf{C}^{[s]}, \mathbf{p}^{[s]}; \psi) - \mu^2(\mathbf{M}^{[s]}, \mathbf{C}^{[s]}, \mathbf{p}^{[s]}; \psi) - \sigma^2(\mathbf{M}^{[s]}, \mathbf{C}^{[s]}, \mathbf{p}^{[s]}; \psi) \right) \right). \quad (18)$$

3) Overall Learning Objective: The overall learning objective jointly optimizes the conditional flow matching loss \mathcal{L}_{CFM} in (16) and the modality alignment loss \mathcal{L}_{MA} in (17) to achieve robust and efficient sensing-to-channel evolution. The associated optimization problem is formulated as

$$\min_{\psi, \theta, \tau} (\mathcal{L}_{\text{CFM}} + \mathcal{L}_{\text{MA}}), \quad (19)$$

which enables joint end-to-end optimization of the multimodal encoder q_{ψ} and the neural velocity field v_{θ} .

B. Model Architecture and Parameterization

This section details the network architectures that implement the overall learning objective in (19), which comprise the multimodal stochastic encoder q_{ψ} that fuses heterogeneous sensing modalities into a latent distribution in channel space, and the neural velocity field v_{θ} for flow matching.

1) Multimodal Stochastic Encoder: The stochastic encoder $q_{\psi}(\cdot)$ employs modality-specific backbone networks to extract multimodal sensing features, and then fuses them into a latent distribution within the channel space.

As detailed in Fig. 3, the encoder integrates three backbone networks – a convolutional neural network (CNN), a point cloud network (PointNet), and a multilayer perceptron (MLP) – to extract features from the image, point cloud, and coordinates, respectively.² Specifically, **(i) the CNN architecture**

²We use three different backbone networks because the three input modalities exhibit fundamentally different structural properties. Specifically, images have 2D spatial correlations suited for the CNN with local-receptive-field capability; point clouds are unordered point sets requiring permutation-invariant models like PointNet; and coordinates are low-dimensional continuous vectors best handled by simple MLPs. If a single network were forced to handle all modalities, it would destroy the inherent structure of each modality, which ultimately leads to a significant degradation in model performance.

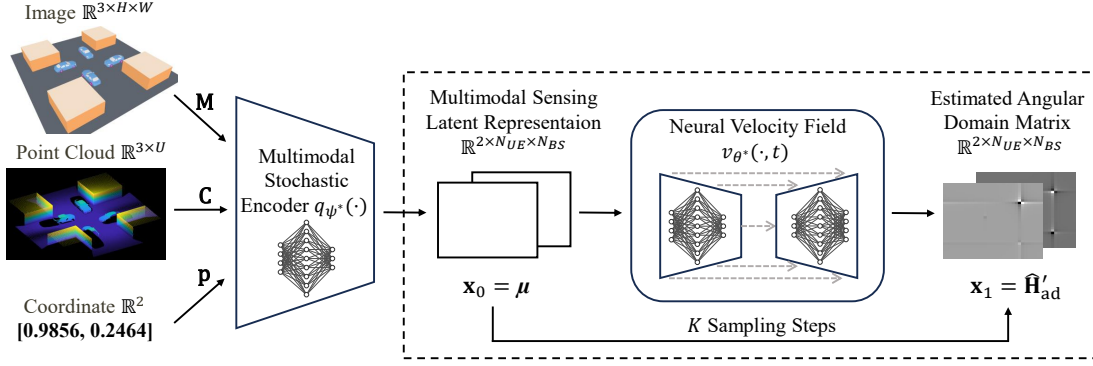


Fig. 5. Inference pipeline that enables the cross-modality evolution from multimodal sensing data to wireless channel representation.

Algorithm 1 Training Cross-Modal Flow Matching for Channel Inference

Require: Training dataset $\mathcal{D} = \{\mathbf{M}^{[s]}, \mathbf{C}^{[s]}, \mathbf{p}^{[s]}, \mathbf{H}_{\text{ad}}^{[s]}\}_{s=1}^S$.

- 1: Initialize batch size B_s , learning rate η , weight λ , number of training epoch N_{tr} .
- 2: Randomly initialize the multimodal stochastic encoder, the neural velocity field and the temperature coefficient with $\psi^{(0)}$, $\theta^{(0)}$ and $\tau^{(0)}$, respectively.
- 3: **for** $n = 1$ to N_{tr} epochs **do**
- 4: Randomly extract a subset $\mathcal{D}_s \subset \mathcal{D}$ with B_s data samples and independently sample B_s time indices $\{t^{[s]}\}_{s=1}^{B_s}$ from the uniform distribution $\mathcal{U}[0, 1]$.
- 5: Compute the mini-batch estimate of the loss in (19) using the sampled subset \mathcal{D}_s and time indices $\{t^{[s]}\}$, and obtain the updated parameters $\psi^{(n)}$, $\theta^{(n)}$, and $\tau^{(n)}$ via Adam with learning rate η .
- 6: **end for**
- 7: **return** Optimized parameters $\psi^* = \psi^{(N_{tr})}$ and $\theta^* = \theta^{(N_{tr})}$.

consists of three stacked 2D convolutional (Conv2D) layers with progressively doubled channel sizes, where each layer halves the spatial resolution via a stride-2 downsampling operation. The resultant feature map from the final Conv2D layer is flattened into a vector, and then processed by a fully-connected (FC) layer to produce a feature vector; **(ii) the PointNet architecture** applies three stacked 1D convolutional (Conv1D) layers to expand the dimensionality of each 3D point, followed by a max-pooling operation across the point dimension to obtain a global feature vector, which is subsequently refined by an FC layer; **(iii) the MLP architecture** applies a sinusoidal encoding module [35] to transform the coordinate into a high-dimensional position embedding, followed by two sequential FC layers that generate the corresponding feature vector.

The resultant modality-specific feature vectors are then concatenated and fused through a multi-head attention layer [12]. The fused feature vector is reshaped into a dual-channel feature map, which is processed by two independent Conv2D layers to produce a mean of $\mu \in \mathbb{R}^{2 \times N_{UE} \times N_{BS}}$ and a log-variance of $\sigma_{\log} \in \mathbb{R}^{2 \times N_{UE} \times N_{BS}}$, respectively. The variance is obtained via $\sigma^2 = \exp(\sigma_{\log})$, which ensures its positivity and thus enhances numerical stability during model training and inference.

Algorithm 2 Pipeline for Online Channel Inference

Require: The integration step number K , the RGB image \mathbf{M} , the point cloud \mathbf{C} , the position coordinate \mathbf{p} , and the learned model parameters ψ^* and θ^* .

- 1: Feed \mathbf{M} , \mathbf{C} , and \mathbf{p} into the multimodal stochastic encoder q_{ψ^*} to obtain the mean μ , and set the initial state to $\mathbf{x}_0 = \mu$.
- 2: Initialize the intermediate state \mathbf{x}_k at $k = 0$ via (22).
- 3: **for** $k = 1$ to $K - 1$ **do**
- 4: Update the intermediate state \mathbf{x}_{kh} to $\mathbf{x}_{(k+1)h}$ via (21).
- 5: **end for**
- 6: Extract the terminal state as estimated channel $\hat{\mathbf{H}}'_{\text{ad}} \leftarrow \mathbf{x}_1$.
- 7: Convert $\hat{\mathbf{H}}'_{\text{ad}}$ into complex-valued form $\hat{\mathbf{H}}_{\text{ad}}$ using Eq. (4), and then transform it into spatial domain $\hat{\mathbf{H}}$ via Eq. (5).
- 8: **return** Estimated channel coefficient matrix $\hat{\mathbf{H}}$.

2) *Neural Velocity Field*: The neural velocity field $v_{\theta}(\cdot, t)$ is designed for predicting the current velocity field from the intermediate state \mathbf{x}_t during flow matching. The U-Net architecture of [36] fits this task well due to its symmetric encoder-decoder design, which preserves spatial dimension between the input and output, while enabling multi-scale feature extraction and flexible conditional information injection. Motivated by these properties, we extend the classic U-Net by incorporating the time step t as an additional conditioning input for flow matching.

As illustrated in Fig. 4, the network consists of an encoding path, a bottleneck block, and a decoding path connected through skip connections. The time step t is first transformed into a high-dimensional embedding using a sinusoidal encoding module [35] and injected into each block via FC projections. **(i) Encoding path**: The intermediate state \mathbf{x}_t is progressively downsampled through encoder blocks, where time embeddings are added to feature maps before applying Conv2D and stride-2 downsampling operations. **(ii) Bottleneck block**: The lowest-resolution feature map is fused with the time embedding and processed by stacked Conv2D layers to capture global context. **(iii) Decoding path**: The feature map is upsampled through decoder blocks that concatenate skip connections from the corresponding encoder layers, integrate time embeddings, and apply Conv2D layers followed by upsampling to restore spatial resolution. The final output $v_{\theta}(\mathbf{x}_t, t)$ represents the predicted velocity field at time step t .

C. Training and Inference Procedures

The parameters of the multimodal stochastic encoder ψ and the neural velocity field θ , as well as the temperature coefficient τ are jointly optimized with the overall learning objective (19). In this paper, we opt for the adaptive moment estimation (Adam) method as the gradient-descent optimizer, because it offers fast and stable convergence by adaptively adjusting per-parameter learning rates. The training process is detailed in Algorithm 1.

With the learned parameters ψ^* and θ^* , Fig. 5 shows the pipeline for estimating the wireless channel from multimodal sensing data. During channel inference, the multimodal stochastic encoder q_{ψ^*} encodes the RGB image \mathbf{M} , the point cloud \mathbf{C} , and the position coordinate \mathbf{p} into the mean $\boldsymbol{\mu}$ and the variance $\boldsymbol{\sigma}$. Whilst the initial state is reparameterized via (15) during training, we adopt a maximum-a-posteriori (MAP) deterministic initialization during inference by setting the initial state to the mode of the multivariate Gaussian distribution, i.e., $\mathbf{x}_0 = \boldsymbol{\mu}$. This strategy eliminates sampling-induced variability, thereby yielding more stable and accurate point estimates for CSI acquisition. To achieve the terminal state, we integrate the ODE in (7) from $t = 0$ to $t = 1$, where the true velocity field $u(\mathbf{x}_t, t)$ is replaced by the learned neural velocity field $v_{\theta}(\mathbf{x}_t, t)$. In practice, the integration interval $t \in [0, 1]$ is discretized into K steps with step size $h = 1/K$. Over each step k , we have

$$\begin{aligned} \mathbf{x}_{(k+1)h} - \mathbf{x}_{kh} &= \int_{kh}^{kh+h} v_{\theta^*}(\mathbf{x}_t, t) dt, \\ &\approx h v_{\theta^*}(\mathbf{x}_{kh}, kh), \end{aligned} \quad (20)$$

which corresponds to the first-order (forward Euler) update.

To improve the numerical accuracy of the integration, we adopt the second-order Adams-Bashforth method [37]. The update for $k = 1, \dots, K-1$ is given by

$$\mathbf{x}_{(k+1)h} = \mathbf{x}_{kh} + h \cdot \left(\frac{3}{2} v_{\theta^*}(\mathbf{x}_{kh}, kh) - \frac{1}{2} v_{\theta^*}(\mathbf{x}_{(k-1)h}, (k-1)h) \right), \quad (21)$$

with the initialization at $k = 0$ as

$$\mathbf{x}_h = \mathbf{x}_0 + h \cdot v_{\theta^*}(\mathbf{x}_0, 0). \quad (22)$$

After K update steps, we obtain the estimated angular-domain channel matrix $\widehat{\mathbf{H}}'_{\text{ad}}$, i.e., the terminal state \mathbf{x}_1 . This estimate is then converted to the complex-valued form $\widehat{\mathbf{H}}_{\text{ad}}$ via (4) and finally mapped to the spatial domain $\widehat{\mathbf{H}}$ via (5). The overall inference procedure is summarized in Algorithm 2.

V. EXPERIMENTAL RESULTS

We employ the NVIDIA Sionna link-level testbench [30] and the Blender graphics suite [31] as our simulators to generate 3GPP-compliant MIMO channels and multimodal sensing data. As shown in Fig. 6, we simulate an urban intersection scenario consisting of four buildings and four moving vehicles, representing the static and dynamic components of the environment, respectively. Specifically, we randomly sample 6,000 user locations and, for each location, simulate the vehicles moving across 5 transmission frames that the user communicates with a central BS, resulting in a dataset of $S = 30,000$ synchronized channel-sensing samples. Both

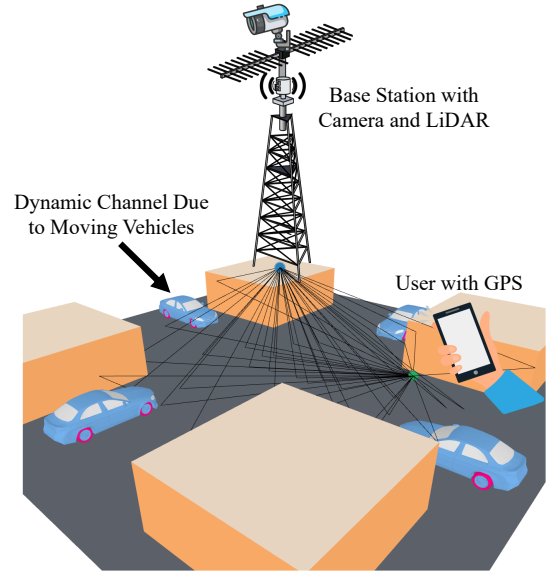


Fig. 6. Illustration of the scene simulated by Sionna and Blender.

the user and the BS employ hybrid analog and digital antenna arrays. The number of antennas is set to $N_{BS} = 64$ and $N_{UE} = 16$, and the corresponding number of RF chains is $N_{RF}^{BS} = 4$ and $N_{RF}^{UE} = 4$. Moreover, the transmission frame period is set to $T_f = 10$ ms and the communication bandwidth is configured as $W = 120$ kHz, resulting in $N_{sym} = 1120$ transmit symbols per frame according to the 5G standard [38].

The proposed cross-modal flow matching framework is implemented in PyTorch and trained on an NVIDIA GeForce RTX 4090 24 GB GPU. The dataset collected is divided into training and testing sets with a 9:1 ratio. The model is trained for $N_{tr} = 2000$ epochs using a batch size of $B_s = 128$. The weight of regularization term is $\lambda = 10^{-4}$ and the learning rate of the Adam optimizer is set to $\eta = 10^{-4}$.

1) **Benchmarks:** To evaluate the proposed framework, we compare it to representative benchmark methods. The first three benchmarks correspond to pilot-based channel estimation approaches. For these methods, the CSI acquisition period T_{ca} is partitioned into two parts: the first $(T_{ca} - T_{ce})$ for pilot transmission and the remaining T_{ce} for executing channel estimation algorithms. This implies that the number of pilot symbols used for channel estimation is given by $(T_{ca} - T_{ce})/T_f \times N_{sym}$.

- **LS-Based Channel Estimation [39]:** The least-squares (LS) method is employed to estimate the channel coefficient matrix directly from the received pilot signals.

- **LASSO-Based Channel Estimation [3]:** The LASSO estimator is applied to estimate the angular-domain channel matrix from the received pilots, which is then transformed back into the spatial domain.

- **Diffusion-Based Channel Estimation [10]:** A diffusion model is pretrained on angular-domain channels to serve as a generative prior. During inference, the model is initialized with Gaussian noise and iteratively refines the noisy sample based on posterior scores computed from both the pretrained prior and the received pilots. This process produces an estimated channel realization in the angular domain, which is

subsequently transformed back into the spatial domain.

We further consider a benchmark that realizes environment-aware channel inference based on the user's location.

- **KNN-Based Channel Inference [14]:** The channels generated by Sionna are represented using a ray-tracing model characterized by the path gain, phase, and zenith/azimuth angles of departure (AoDs) and arrival (AoAs). For each user location, the three strongest propagation paths are first selected from each transmission frame. The corresponding channel parameters are then averaged across five consecutive frames to obtain three representative paths. Based on the training samples, an inverse-distance-weighted KNN algorithm is employed to predict the path parameters at unseen locations according to their spatial proximity to the training locations, which are subsequently used for reconstructing the channel coefficient matrix.

The aforementioned benchmarks are also extended to downstream physical-layer operations that rely on CSI, among which we specifically consider beamforming design in our experiments and include the following task-oriented benchmark.

- **Multimodal-Sensing-Aided Beam Selection [12]:** The method in [12] considers a multiple-input single-output (MISO) system using a fully digital antenna array. To adapt it to our MIMO setting with hybrid analog-digital arrays, we construct DFT codebooks for the analog transmit precoder (TPC) and receive combiner (RC), and Grassmannian codebooks for their digital counterparts. A Transformer network is then employed to infer the optimal beam indices in these codebooks from multimodal sensing inputs (RGB image, LiDAR point cloud, and user coordinate). The final hybrid TPC and RC are obtained by combining the selected analog and digital components.

2) *Evaluation Metrics:* Given the estimated channel matrix $\widehat{\mathbf{H}}^{[i]}$ and its ground-truth $\mathbf{H}^{[i]}$ at the i -th transmission frame, the channel estimation accuracy is evaluated using the normalized mean square error (NMSE), defined as

$$(\text{NMSE}) \quad \frac{\|\mathbf{H}^{[i]} - \widehat{\mathbf{H}}^{[i]}\|_F^2}{\|\mathbf{H}^{[i]}\|_F^2}, \quad (23)$$

While NMSE quantifies the element-wise estimation error, we also consider the cosine similarity for richer characterization. This metric quantifies the alignment between the subspaces spanned by the estimated and ground-truth channel matrices, which is particularly relevant for beamforming-oriented tasks:

$$(\text{Cosine Similarity}) \quad \frac{\|(\mathbf{H}^{[i]})^H \widehat{\mathbf{H}}^{[i]}\|_F}{\|\mathbf{H}^{[i]}\|_F \|\widehat{\mathbf{H}}^{[i]}\|_F}. \quad (24)$$

Both metrics are averaged over all transmission frames and user locations.

To evaluate the beamforming performance, we consider the achievable spectral efficiency (SE), which depends on the channel acquisition time duration T_{ca} . Explicitly, T_{ca} is defined as the duration from the beginning of channel acquisition until the beam selection is completed. Although this definition slightly extends the conventional notion of channel acquisition, it captures the total latency in inferring the beamforming vectors. For fair comparison, we use the same analog and

TABLE II
ABLATION STUDY ON TRAINING OBJECTIVES

Metric \ Loss	Loss		
	CFM	CFM+Recon	CFM+MA
NMSE (dB)	-4.86	-5.78	-10.21
Cosine Similarity	0.82	0.86	0.95

[†]The number of numerical integration steps is $K = 7$.

digital codebooks as those in the multimodal-sensing-aided beam selection benchmark, and adopt the two-stage search algorithm [40] to obtain the hybrid TPC $\widehat{\mathbf{F}}^{[i]} \in \mathbb{C}^{N_{BS} \times 1}$ and RC $\widehat{\mathbf{W}}^{[i]} \in \mathbb{C}^{N_{UE} \times 1}$ that align with the dominant spatial direction of the channel. Accordingly, the instantaneous SE is

$$R(\widehat{\mathbf{W}}^{[i]}, \widehat{\mathbf{F}}^{[i]}, \mathbf{H}^{[i]}) = \log_2 \left(1 + \gamma_{SNR} \left| (\widehat{\mathbf{W}}^{[i]})^H \mathbf{H}^{[i]} \widehat{\mathbf{F}}^{[i]} \right|^2 \right), \quad (25)$$

where γ_{SNR} is the signal-to-noise ratio (SNR).

In pilot-based channel estimation schemes, both pilot signaling and CSI recovery are performed within the channel acquisition period T_{ca} , during which no data transmission occurs. The resultant effective achievable SE within one frame is given by

$$(\text{Pilot-Based SE}) \quad \frac{T_f - T_{ca}}{T_f} R(\widehat{\mathbf{W}}^{[i]}, \widehat{\mathbf{F}}^{[i]}, \mathbf{H}^{[i]}). \quad (26)$$

By contrast, in environment-aware and sensing-aided communications, as illustrated in Fig. 2, the computation processes for the current frame are performed concurrently with data transmission using the beamformers from the previous frame. The average achievable SE within a frame is therefore calculated as

$$(\text{Sensing-Aided SE}) \quad \frac{T_{ca}}{T_f} R(\widehat{\mathbf{W}}^{[i-1]}, \widehat{\mathbf{F}}^{[i-1]}, \mathbf{H}^{[i]}) - \frac{128 \text{ bits}}{T_f W} + \frac{T_f - T_{ca}}{T_f} R(\widehat{\mathbf{W}}^{[i]}, \widehat{\mathbf{F}}^{[i]}, \mathbf{H}^{[i]}), \quad (27)$$

where the second term represents the overhead associated with GPS query, assuming that 128 bits are used to encode the two-dimensional user coordinate. All metrics are averaged over the last four transmission frames, excluding the first frame to avoid the ambiguity of channel initialization, and over all user locations.

A. Ablation and Parameter Study

We conduct an ablation study on the training objectives to justify the rationale for including the modality alignment loss. Three configurations are compared: the baseline CFM model trained solely with the flow matching loss; the CFM+Recon variant, which incorporates a reconstruction loss following [28], where modality-specific decoders reconstruct each modality from the shared latent representation, thereby introducing both the reconstruction loss and the KL regularization; and the proposed CFM+MA scheme that jointly optimizes the CFM and modality alignment losses for efficiently bridging the source and target distributions. In this experiment, the number of integration steps is fixed at $K = 7$. As summarized in Table II, the CFM+MA scheme achieves

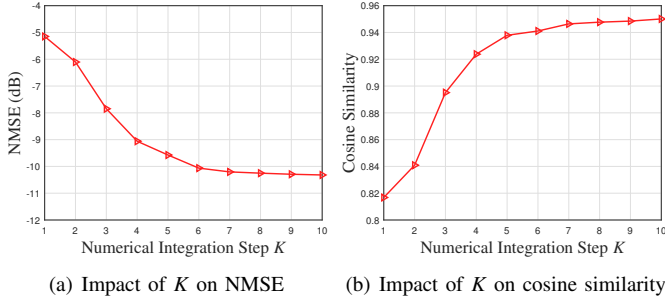


Fig. 7. The impact of numerical integration step K on channel estimation quality.

the best overall performance, yielding an NMSE of -10.21 dB and a cosine similarity of 0.95. In simple tangible terms, this represents an approximately factor 10 reduction attainable by harnessing our proposed technique. The baseline CFM exhibits the worst estimation quality, with an NMSE of -4.86 dB and a cosine similarity of 0.82, while the CFM+Recon configuration moderately improves the performance to -5.78 dB NMSE and 0.86 cosine similarity. These results suggest that, compared with merely preserving multimodal information in the latent space as in the CFM+Recon scheme, directly enforcing alignment between the source and target distributions shortens the transport path and thus enhances channel estimation accuracy.

We study the impact of the number of numerical integration steps K used during inference regardless of the latency constraint, which determines the discretization resolution of the flow-matching process. As shown in Fig. 7, the channel estimation performance improves as K increases, with the NMSE decreasing and the cosine similarity increasing due to the reduced numerical integration error. However, when K exceeds 7, further increasing it to 10 yields only a marginal NMSE improvement of 0.5 dB and approximately 0.01 in cosine similarity gain. This indicates that the discrete update already provides a sufficiently accurate approximation of the continuous integration process. Based on this observation, we set $K = 7$ as the default value in the following experiments, unless otherwise specified.

Fig. 8 illustrates the cross-modality evolution process from the latent multimodal sensing representation to the angular-domain channel matrix during inference. As the evolution proceeds, the channel estimation quality shows a steady improvement. At the initial step ($k = 0$), the latent representation is unstructured, yielding a high NMSE of 28.43 dB and a low cosine similarity of 0.10. As the neural ODE is numerically integrated forward, i.e., as k increases, the NMSE gradually decreases while the cosine similarity increases, with the sparsity pattern of the angular-domain channel progressively emerging. Upon completing the integration at $k = 7$, the estimated angular-domain channel matrix (i.e., the terminal state) clearly exhibits a sparsity pattern similar to that of the ground truth in Fig. 8(f), achieving an NMSE of -10.25 dB and a cosine similarity of 0.96.

The number of numerical integration steps K directly influences the inference latency of the proposed cross-modal flow

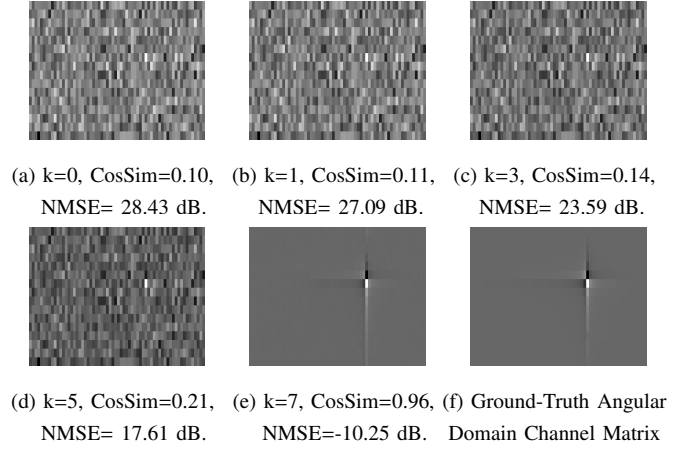


Fig. 8. Cross-modality evolution process from the multimodal sensing latent representation to the angular-domain channel matrix.

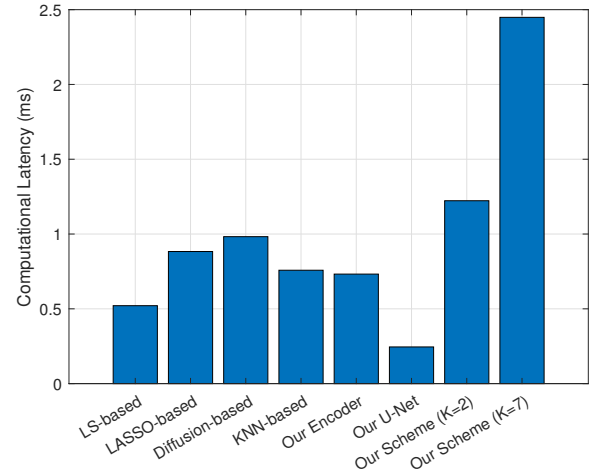
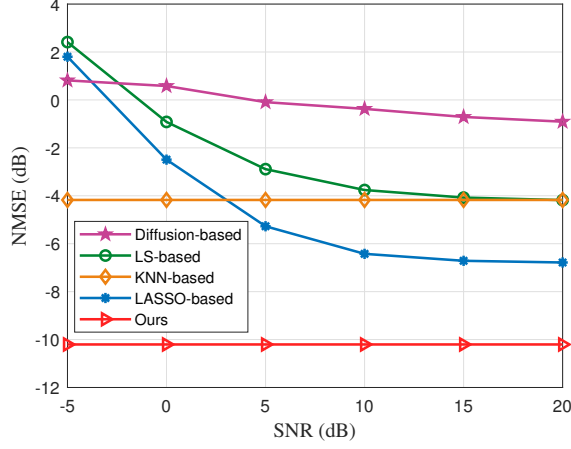
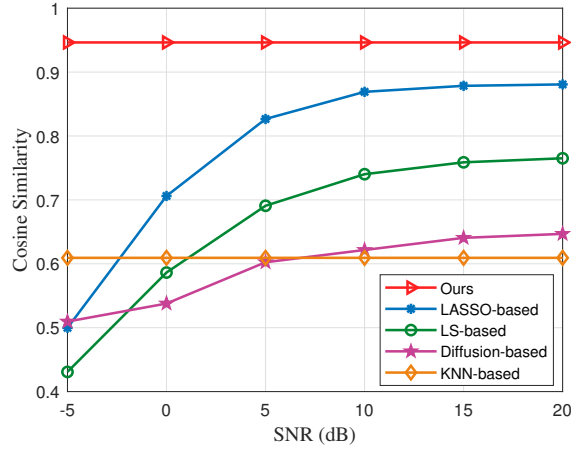


Fig. 9. Computational latency comparison of sensing-aided channel inference and pilot-based channel estimation schemes.

matching framework. Accordingly, Fig. 9 reports the end-to-end computational latency of all the channel estimation and inference schemes considered. In our framework, the multimodal stochastic encoder is activated once per inference, requiring approximately 0.75 ms, while the U-Net is harnessed K times, with an average runtime of 0.25 ms per step. Consequently, the total inference latency is about 1.25 ms for $K = 2$ and 2.5 ms for $K = 7$. For the pilot-based channel estimation schemes (LS, LASSO, and diffusion), the conventional computing time corresponds to the processing latency from pilot reception to channel estimation. Although these methods achieve sub-millisecond computation time, motivating the setting of $T_{ce} = 1$ ms in the following experiments, the overall channel acquisition duration also includes pilot transmission, which plays a similar role to the inference process in our framework. Even at the maximum integration step ($K = 7$), the inference latency of our method remains below 2.5 ms, which is comparable to the typical CSI acquisition period. Considering that the GPS query times are negligible, the proposed framework fully satisfies the latency constraints of 5G communication systems.



(a) Impact of SNR on NMSE

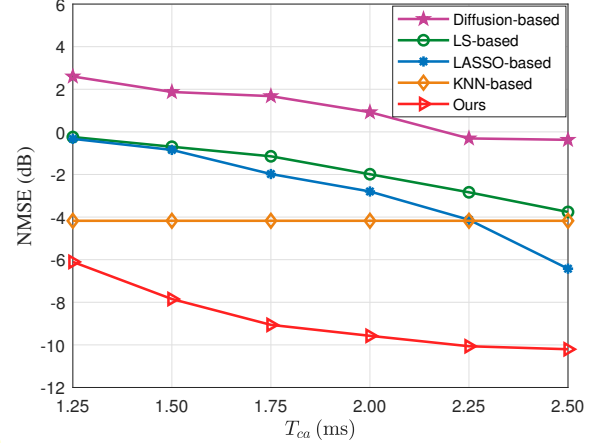
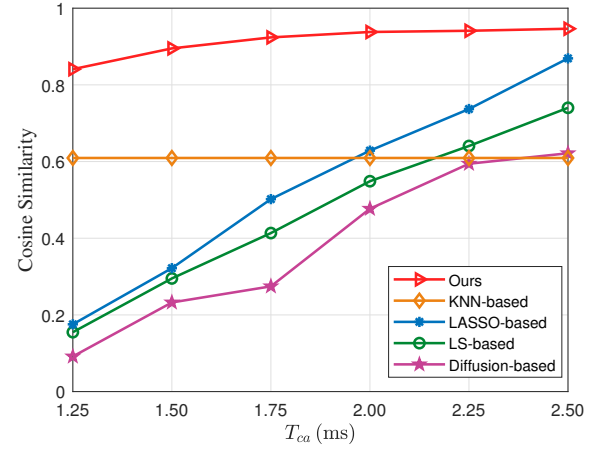


(b) Impact of SNR on cosine similarity

Fig. 10. The impact of SNR on channel estimation quality under the CSI acquisition period $T_{ca} = 2.5$ ms.

B. Channel Estimation Performance versus SNR

In Fig. 10(a) and Fig. 10(b), we investigate the effect of SNR on NMSE and cosine similarity, respectively, and compare our scheme to different CSI acquisition methods. In this experiment, the CSI acquisition period is set to $T_{ca} = 2.5$ ms. It is observed that our proposed method achieves the lowest NMSE and the highest cosine similarity among all the schemes. Another observation is that the performance of our proposed scheme and of the KNN-based channel inference scheme is almost invariant to SNR. This is because sensing-aided methods estimate CSI directly from environmental sensing data rather than relying on noisy pilot observations, which makes them robust to time-variant SNR levels. Although the KNN-based method achieves lower computational latency (as shown in Fig. 9), the experimental result seen in Fig. 10(a) and Fig. 10(b) demonstrates that its estimation quality is much worse than that of our scheme, since it only exploits user location and ignores the real-time dynamics of the wireless environment. By contrast, for all pilot-based channel estimation schemes, the performance improves upon increasing the SNR, as higher

(a) Impact of T_{ca} on NMSE(b) Impact of T_{ca} on cosine similarityFig. 11. The impact of CSI acquisition period T_{ca} on channel estimation quality under the SNR = 10 dB. The numerical integration step K varies with T_{ca} .

SNR leads to reduced pilot contamination by channel noise. However, in the high-SNR regime, their performance becomes limited by the number of available pilots, rather than by pilot quality. Although the diffusion model theoretically provides a strong generative prior for channel estimation with limited pilots, the strict latency constraint prevents sufficient iterative refinement, leading to even worse performance than classical LS and LASSO estimators.

C. Channel Estimation Performance versus CSI Acquisition Period

Fig. 11(a) and Fig. 11(b) plot the NMSE and cosine similarity versus the CSI acquisition time. In this experiment, the SNR is fixed at 10 dB, and the CSI acquisition period T_{ca} varies from 1.25 ms to 2.5 ms, corresponding to the number of numerical integration steps K increasing from 2 to 7 in our scheme. The results show that the proposed scheme consistently outperforms all benchmark methods across the considered range of CSI acquisition period. For the KNN-based method, the inference time lies at the lower bound

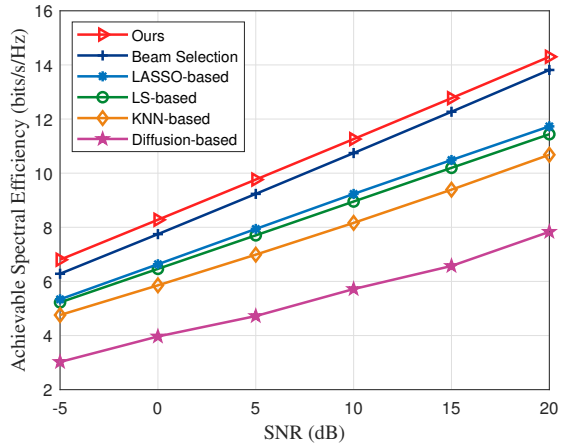


Fig. 12. The impact of SNR on achievable SE under the CSI acquisition period $T_{ca} = 2.5$ ms.

of the range considered (i.e., $T_{ca} = 1.25$ ms), hence increasing the CSI acquisition period does not contribute to further performance gains. BY contrast, all pilot-based channel estimation schemes benefit from longer CSI acquisition period, since more pilots can be transmitted for reducing the channel estimation error.

D. Achievable SE versus SNR and CSI Acquisition Period

In Fig. 12, we evaluate the impact of SNR on the achievable SE for the hybrid beamforming task under different channel acquisition schemes, including both pilot-based channel estimation and sensing-aided channel inference methods. The channel acquisition period is set to $T_{ca} = 2.5$ ms. As shown in the figure, the proposed method consistently outperforms all benchmark schemes across the SNR range considered. Compared to conventional pilot-based channel estimation schemes (LS, LASSO, and diffusion), the performance gain arises from two factors: improved channel estimation accuracy and the ability to reuse the channel acquisition time for data transmission, thereby enhancing the overall spectral efficiency by reducing the pilot overhead through computation. Moreover, the SE improvement over the KNN-based channel inference scheme arises from more accurate channel inference in dynamic environments enabled by sensing environmental variations. While the multimodal sensing-aided beam selection method can also adapt to environmental dynamics, our scheme leverages the full CSI and thus yields more precise and stable beamforming decisions, leading to further SE gains.

Fig. 13 illustrates the impact of the CSI acquisition period T_{ca} on the achievable SE, where the SNR is fixed at 10 dB. The SE of the proposed scheme first increases and then shows a slight degradation as T_{ca} becomes larger. The initial improvement comes from more accurate CSI enabled by increasing the number of numerical integration steps K ; however, once the accuracy saturates at large T_{ca} (see Fig. 11), the loss caused by outdated CSI begins to dominate the performance, while the improved CSI accuracy only provides marginal SE gain. By contrast, the SE of the multimodal sensing-aided beam selection scheme decreases almost linearly with T_{ca} ,

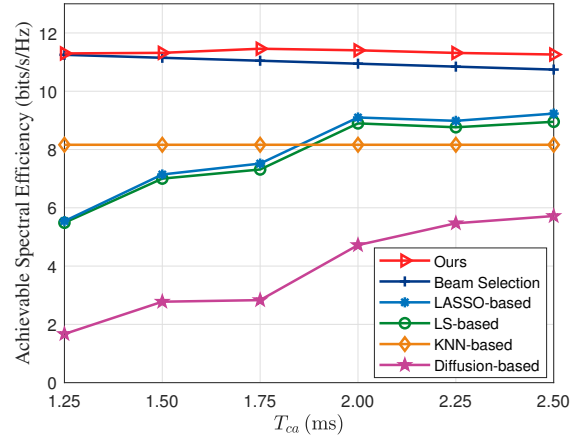


Fig. 13. The impact of CSI acquisition period T_{ca} on achievable SE under the SNR = 10 dB. The numerical integration step K varies with T_{ca} .

since longer acquisition periods cause a larger portion of the data transmission to rely on outdated CSI. The achievable SE of the KNN-based scheme remains constant for all T_{ca} values, as the beam selection does not change once the user's location is fixed. This can also be confirmed from (27). For the pilot-based channel estimation schemes (LS, LASSO, and diffusion), within the smaller T_{ca} regime, the SE increases with the improved channel estimation accuracy, but eventually saturates, once the channel estimation is sufficiently accurate.

VI. CONCLUSIONS

A novel framework was conceived for environment-aware channel inference that estimates the complete CSI directly from multimodal sensing data without relying on pilot signaling. By formulating the channel inference task as a cross-modal flow matching problem, the proposed method bridges the distributions of multimodal sensing inputs and channel representations through a learned continuous flow. A stochastic encoder and a neural velocity field were jointly optimized using the conditional flow matching and modality alignment losses to ensure tractable learning. The channel inference is represented as an ODE integration process, where a second-order numerical scheme enables real-time and model-free CSI estimation. System-level evaluations verify that the proposed framework consistently outperforms both pilot-based and existing sensing-based baselines in estimation accuracy and downstream beamforming tasks.

This work serves as an important step toward environment-aware NG communications. As an extension of the current study, it is important to further reduce the channel inference latency by employing a single-step numerical integration scheme in the proposed framework, while preserving the CSI estimation quality. This improvement is particularly critical in high-mobility networks (e.g., vehicular or high-speed railway scenarios), where the channel coherence time is significantly shorter. Another interesting direction is to investigate environment-aware channel inference in real-world scenarios, where the sensing modalities provide only a partial environmental observation due to limited sensor resolution,

occlusions and calibration errors. Consequently, the same observed modalities may correspond to multiple plausible propagation conditions. This naturally motivates unlocking the probabilistic generation capability of our framework to sample diverse channel realizations consistent with the sensed data. By explicitly capturing such uncertainty, the communication system can design more robust strategies for downstream tasks such as beamforming, link adaptation, and resource allocation.

REFERENCES

- [1] C.-X. Wang, X. You, X. Gao, X. Zhu, Z. Li, C. Zhang, H. Wang, Y. Huang, Y. Chen, H. Haas, J. S. Thompson, E. G. Larsson, M. D. Renzo, W. Tong, P. Zhu, X. Shen, H. V. Poor, and L. Hanzo, "On the road to 6G: Visions, requirements, key technologies, and testbeds," *IEEE Commun. Surv. Tutorials*, vol. 25, no. 2, pp. 905–974, 2023.
- [2] Z. Wang, J. Zhang, H. Du, D. Niyato, S. Cui, B. Ai, M. Debbah, K. B. Letaief, and H. V. Poor, "A tutorial on extremely large-scale MIMO for 6G: Fundamentals, signal processing, and applications," *IEEE Commun. Surv. Tutorials*, vol. 26, no. 3, pp. 1560–1605, 2024.
- [3] P. Schniter and A. Sayeed, "Channel estimation and precoder design for millimeter-wave communications: The sparse way," in *Proc. 48th Asilomar Conf. Signals, Syst., Comput.*, 2014, pp. 273–277.
- [4] P. Schniter and S. Rangan, "Compressive phase retrieval via generalized approximate message passing," *IEEE Trans. Signal Process.*, vol. 63, no. 4, pp. 1043–1055, 2015.
- [5] B. Zhou, X. Yang, S. Ma, F. Gao, and G. Yang, "Low-overhead channel estimation via 3D extrapolation for TDD mmwave massive MIMO systems under high-mobility scenarios," *IEEE Trans. Wireless Commun.*, vol. 24, no. 4, pp. 2797–2813, 2025.
- [6] B. Zhou, X. Yang, S. Ma, F. Gao, and G. Yang, "Pay less but get more: A dual-attention-based channel estimation network for massive MIMO systems with low-density pilots," *IEEE Trans. Wireless Commun.*, vol. 23, no. 6, pp. 6061–6076, 2024.
- [7] Z. Chen, Z. Zhang, Z. Yang, C. Huang, and M. Debbah, "Channel deduction: A new learning framework to acquire channel from outdated samples and coarse estimate," *IEEE J. Sel. Areas Commun.*, vol. 43, no. 3, pp. 944–958, 2025.
- [8] L. Shi, J. Zhang, L. Yu, Y. Zhang, Z. Zhang, Y. Cai, and G. Liu, "Can wireless environment information decrease pilot overhead: A channel prediction example," *IEEE Wireless Commun. Lett.*, vol. 14, no. 3, pp. 861–865, 2025.
- [9] M. Arvinte and J. I. Tamir, "MIMO channel estimation using score-based generative models," *IEEE Trans. Wireless Commun.*, vol. 22, no. 6, pp. 3698–3713, 2023.
- [10] X. Zhou, L. Liang, J. Zhang, P. Jiang, Y. Li, and S. Jin, "Generative diffusion models for high dimensional channel estimation," *IEEE Trans. Wireless Commun.*, pp. 1–15, 2025.
- [11] Y. Zeng, J. Chen, J. Xu, D. Wu, X. Xu, S. Jin, X. Gao, D. Gesbert, S. Cui, and R. Zhang, "A tutorial on environment-aware communications via channel knowledge map for 6G," *IEEE Commun. Surv. Tutorials*, vol. 26, no. 3, pp. 1478–1519, 2024.
- [12] Y. Cui, J. Nie, X. Cao, T. Yu, J. Zou, J. Mu, and X. Jing, "Sensing-assisted high reliable communication: A Transformer-based beamforming approach," *IEEE J. Sel. Top. Signal Process.*, vol. 18, no. 5, pp. 782–795, 2024.
- [13] G. Charan and A. Alkhateeb, "Computer vision aided blockage prediction in real-world millimeter wave deployments," in *Proc. IEEE Globecom Workshops (GC Wkshps)*, 2022, pp. 1711–1716.
- [14] D. Wu, Y. Zeng, S. Jin, and R. Zhang, "Environment-aware and training-free beam alignment for mmwave massive MIMO via channel knowledge map," in *Proc. IEEE Int. Conf. Commun. Workshops (ICC Workshops)*, 2021, pp. 1–7.
- [15] X. Zhao, Z. An, Q. Pan, and L. Yang, "NeRF2: Neural radio-frequency radiance fields," in *Proc. ACM Int. Conf. Mobile Comput. Netw. (MobiCom)*, Madrid, Spain, 2023.
- [16] K. Wang, L. Yu, J. Zhang, Y. Tian, E. Guo, and G. Liu, "Multi-modal environmental information sensing based path loss prediction for V2I communications," in *Proc. IEEE 101st Veh. Technol. Conf. (VTC2025-Spring)*, 2025, pp. 1–5.
- [17] X. Zhang, R. He, M. Yang, Z. Qi, Z. Zhang, B. Ai, and Z. Zhong, "Vision-aided channel prediction based on image segmentation at street intersection scenarios," *IEEE Trans. Cogn. Commun. Netw.*, 2025.
- [18] Z. Xin, Y. Liu, J. Xing, J. Huang, J. Bian, and Y. Zhang, "A novel multimodal fusion sensing-based channel prediction method for UAV communications," *IEEE Internet Things J.*, vol. 12, no. 4, pp. 3948–3960, 2025.
- [19] Y. Lipman, R. T. Q. Chen, H. Ben-Hamu, M. Nickel, and M. Le, "Flow matching for generative modeling," in *Proc. 11th Int. Conf. Learn. Represent. (ICLR)*, 2023.
- [20] A. Tong, K. FATRAS, N. Malkin, G. Huguette, Y. Zhang, J. Rector-Brooks, G. Wolf, and Y. Bengio, "Improving and generalizing flow-based generative models with minibatch optimal transport," *Trans. Mach. Learn. Res.*, 2023.
- [21] X. Xu, X. Mu, Y. Liu, H. Xing, Y. Liu, and A. Nallanathan, "Generative artificial intelligence for mobile communications: A diffusion model perspective," *IEEE Commun. Mag.*, vol. 63, no. 7, pp. 98–105, 2025.
- [22] G. Liang, J. Hu, K. Yang, S. Song, T. Liu, N. Xie, and Y. Yu, "Data augmentation for predictive digital twin channel: Learning multi-domain correlations by convolutional TimeGAN," *IEEE J. Sel. Top. Signal Process.*, vol. 18, no. 1, pp. 18–33, 2024.
- [23] X. Liu, C. Gong, and Qiang Liu, "Flow straight and fast: Learning to generate and transfer data with rectified flow," in *Proc. 11th Int. Conf. Learn. Represent. (ICLR)*, 2023.
- [24] L. Zhou, A. Lou, S. Khanna, and S. Ermon, "Denoising diffusion bridge models," in *Proc. 12th Int. Conf. Learn. Represent. (ICLR)*, 2024.
- [25] G.-H. Liu, A. Vahdat, D.-A. Huang, E. A. Theodorou, W. Nie, and A. Anandkumar, "I2SB: image-to-image Schrödinger bridge," in *Proc. 40th Int. Conf. Mach. Learn. (ICML)*, Honolulu, Hawaii, USA, 2023.
- [26] X. Yang, C. Cheng, X. Yang, F. Liu, and G. Lin, "Text-to-image rectified flow as plug-and-play priors," in *Proc. 13th Int. Conf. Learn. Represent. (ICLR)*, 2025.
- [27] Y. Luo, D. Du, H. Huang, Y. Fang, and M. Wang, "CurveFlow: Curvature-guided flow matching for image generation," 2025. [Online]. Available: <https://arxiv.org/abs/2508.15093>
- [28] Q. Liu, X. Yin, A. Yuille, A. Brown, and M. Singh, "Flowing from words to pixels: A noise-free framework for cross-modality evolution," in *Proc. IEEE/CVF Conf. Comput. Vis. Pattern Recognit. (CVPR)*, June 2025, pp. 2755–2765.
- [29] J. He, Q. Yu, Q. Liu, and L.-C. Chen, "FlowTok: Flowing seamlessly across text and image tokens," 2025. [Online]. Available: <https://arxiv.org/abs/2503.10772>
- [30] J. Hoydis, S. Cammerer, F. A. Aoudia, A. Vem, N. Binder, G. Marcus, and A. Keller, "Sionna: An open-source library for next-generation physical layer research," 2023. [Online]. Available: <https://arxiv.org/abs/2203.11854>
- [31] Blender Online Community, *Blender - a 3D modelling and rendering package*, Blender Foundation, Amsterdam, The Netherlands, 2018. [Online]. Available: <https://www.blender.org>
- [32] B. Fesl, M. Baur, F. Strasser, M. Joham, and W. Utschick, "Diffusion-based generative prior for low-complexity MIMO channel estimation," *IEEE Wireless Commun. Lett.*, vol. 13, no. 12, pp. 3493–3497, 2024.
- [33] E. Zhu, H. Sun, and M. Ji, "Physics-informed generalizable wireless channel modeling with segmentation and deep learning: Fundamentals, methodologies, and challenges," *IEEE Wireless Commun.*, vol. 31, no. 6, pp. 170–177, 2024.
- [34] A. Radford, J. W. Kim, C. Hallacy, A. Ramesh, G. Goh, S. Agarwal, G. Sastry, A. Askell, P. Mishkin, J. Clark *et al.*, "Learning transferable visual models from natural language supervision," in *Proc. Int. Conf. Mach. Learn. (ICML)*, 2021, pp. 8748–8763.
- [35] A. Vaswani, N. Shazeer, N. Parmar, J. Uszkoreit, L. Jones, A. N. Gomez, L. Kaiser, and I. Polosukhin, "Attention is all you need," in *Proc. 31st Int. Conf. Neural Inf. Process. Syst. (NeurIPS)*, Long Beach, California, USA, 2017, pp. 6000–6010.
- [36] O. Ronneberger, P. Fischer, and T. Brox, "U-Net: Convolutional networks for biomedical image segmentation," in *Proc. Int. Conf. Med. Image Comput. Comput.-Assist. Intervent. (MICCAI)*, Munich, Germany, 2015.
- [37] E. Hairer, G. Wanner, and S. P. Nørsett, *Solving ordinary differential equations I: Nonstiff problems*. Springer, 1993.
- [38] 3GPP, "Radio resource control (RRC) protocol specification," 3rd Generation Partnership Project (3GPP), Technical Specification (TS) 38.331, Jun 2019, version 15.6.0.
- [39] S. M. Kay, *Fundamentals of statistical signal processing: estimation theory*. Prentice-Hall, Inc., 1993.
- [40] K. Satyanarayana, M. El-Hajjar, P.-H. Kuo, A. Mourad, and L. Hanzo, "Dual-function hybrid beamforming and transmit diversity aided millimeter wave architecture," *IEEE Trans. Veh. Technol.*, vol. 67, no. 3, pp. 2798–2803, 2018.